Electron microscopy investigation of iodine intercalated in $Bi_2Sr_2CaCu_2O_x$: Location and ordering of I_3^- molecules

T. Stoto and D. Pooke
New Zealand Institute for Industrial Research, P.O. Box 31-310, Lower Hutt, New Zealand

K. Kishio
Department of Applied Chemistry, University of Tokyo, 7-3-1 Hongo, Bunkyo-ku, Tokyo 113, Japan
(Received 23 August 1994; revised manuscript received 16 January 1995)

The location of I_3^- linear molecules intercalated in $Bi_2Sr_2CaCu_2O_x$ has been determined using electron diffraction and high-resolution electron microscopy observations along the [001] direction. The analysis of short-range-order diffuse scattering and superlattice spots on the diffraction patterns showed that I_3^- units are present in between the facing BiO layers, and that they lie with their long axis parallel to the [010] direction and form locally regular arrangements. The existence of small domains of ordered phases was confirmed by high-resolution microscopy. From these observations a structural model is proposed in which the I_3^- units stack side by side to form zig-zag ribbons extending in the [100] direction. This model can also explain previously reported results and removes the discrepancy between their interpretation.

I. INTRODUCTION

The intercalation of iodine into the Bi-Sr-Ca-Cu-oxide superconductors has received much attention because of the possibilities that this process offered for tuning the superconducting parameters through both structural and electronic modification of the parent phase. Specifically, the intercalation of iodine increases the separation of the CuO_2 planes by 0.35 nm and is also responsible for charge transfer to the CuO_2 planes, with concomitant changes in T_c.[1]

The guest iodine is located between the weakly bound Bi-O bilayers.[2] High-resolution electron microscopy results were originally interpreted on the basis of isolated iodine atoms located between every pair of facing oxygens in the neighboring BiO planes.[3,4] However, Raman measurements[5] showed the presence of linear I_3^- ions, aligned parallel to the a or b axis and placed in sites of low symmetry. Mössbauer measurements[6] confirmed I_3^- as the chemical species of iodine present in the lattice. The structural configuration of triiodide ion chains in the host crystal is still an open problem.

In order to find a model consistent with the different observations, we have carried out a comparative c-axis electron microscopy study of the intercalated and parent phases. Observations along this zone axis, neglected in previous microscopy studies, have revealed not only the location of the linear I_3^- ions, but also the presence of locally ordered iodine structures responsible for short-range-order diffuse scattering and long-range-order superlattice reflections in the electron diffraction patterns.

II. EXPERIMENTAL DETAILS

Single crystals of the $Bi_2Sr_2CaCu_2O_x$ (Bi2212) phase were grown by the floating zone technique in an infrared imaging furnace,[7] using feed rods of cation stoichiometry $Bi_{2.1}Sr_{1.8}CaCu_2$. Samples were intercalated by sealing with elemental iodine in evacuated Pyrex-glass ampoules and annealing at 180 °C for periods of up to two weeks.

TEM foils were prepared in three different ways: argon ion milling, cleavage and crushing in an agate mortar.

Conventional transmission electron microscopy and energy-dispersive spectroscopy (EDS) microanalysis were performed at 100 keV, using a Philips EM400T microscope equipped with an energy-dispersive x-ray-analysis (EDAX) spectrometer. High-resolution observations were carried out at 300 keV, using the Philips EM430ST microscope of the Centre Interdépartemental de Microscopie Electronique, Ecole Polytechnique Fédérale de Lausanne, in Switzerland (point-to-point resolution 0.2 nm and spherical aberration constant 1.2 mm).

Calculations of electron diffraction patterns, modeled supercells and high-resolution electron microscopy (HREM) images were carried out by using the software package EMS.[8] The software SEMPER was employed for filtering the experimental images.[9]

III. RESULTS AND DISCUSSION

Structural considerations

The comparison between x-ray[10] and selected area electron-diffraction patterns of iodine-intercalated and parent Bi2212 phase have shown that the intercalated material has a primitive orthogonal unit cell and that the lattice parameters are $a = b = 0.54$ nm, as in the parent phase, and $c = 1.89$ nm, i.e., 0.35 nm longer than half of the c parameter of the parent phase. The intercalated crystal exhibits an incommensurate modulation along the b axis as in the parent phase.[11] No extinction has been observed.

Electron diffraction: Short-range-order diffuse scattering

In addition to the fundamental Bragg reflections corresponding to this crystal structure, which represent the host material, all the [001] zone axis diffraction patterns of the I-Bi2212 compound contain more or less intense diffuse scattering intensities as shown in Fig. 1. The diffuse scattering features, which are related to short-range order of the intercalated iodine sublattice, are often very weak and appear clearly only on long-exposure patterns. This could be the reason why they had not previously been reported for this compound. Several authors have shown that even the diffuse scattering of x rays is very sensitive to the state of order of intercalated iodine and, in particular, of triiodide ion chains in various compounds.[12–15]

The typical short-range-order (SRO) intensity distribution (Fig. 1) consists of diffuse superlattice reflections, which are split and elongated. An important aspect of this distribution is the existence of a modulation with a period of $1.84\mathbf{b}^*$. In direct space, this corresponds to a distance of about $0.54\mathbf{b}$, or half the length of the triiodide linear chain (about 0.59 nm). This is the signature of the molecular nature of iodine in the host material. In Appendix A it is shown that the observed diffuse scattering can be related to a displacement disorder due to iodine atoms that do not occupy an atomic site corresponding to the space group of the host material. The modulation arises because there exists a spatial correlation between the iodine atoms within an individual chain: the iodine atoms at the ends of the chain are correlated to each other and to the atom at the center of the chain. The periodicity of the modulation is inversely related to the interatomic distance of a correlated pair. This suggests the existence of an arrangement of linear I_3^- molecules all parallel to the b axis with the two iodine atoms at the ends of the chains not lying in one of the atomic sites of the host lattice.

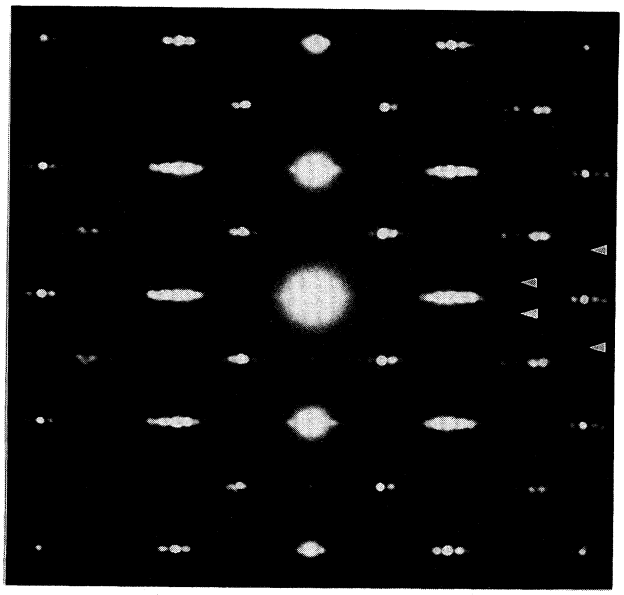

FIG. 1. Typical long-exposure [001] zone axis diffraction patterns observed in single crystals of the I-Bi2212 compound. In addition to the fundamental Bragg reflections corresponding to the crystal structure of the host material, the pattern shows a distribution of diffuse scattering intensities characterized by modulated diffuse superlattice reflections split and elongated along the direction indicated by the short arrows. The period of modulation of the diffuse streaks is $1.84\mathbf{b}^*$.

A model based on arrangements of I_3^- chains parallel to the b axis, with the central atom between two oxygen atoms of facing BiO layers and chain end members slightly displaced with respect to the facing bismuth atoms (because the chain length is a slightly longer than the lattice parameter), is able to explain the modulation of the diffuse scattering intensity distribution. Furthermore, this kind of configuration is also very reasonable from the point of view of the Coulomb interactions and of the atomic radii. The central iodine atom can sit in between two oxygen atoms and, because of its neutrality, behaves covalently (with a radius of 0.133 nm), whereas the iodine atoms at the ends of the chain, which are both charged $-\frac{1}{2}$, have an ionic radius of 0.216 nm and are close to the Bi^+ cations of the neighboring BiO layers.

The diffuse scattering maxima in Fig. 1 are split, indicating the existence of small ordered domains with antiphase boundaries. Appendix B shows that the direction of the splitting, parallel to the a^* axis, is parallel with the normal to the translation interface and the magnitude of the splitting, $\frac{1}{2}a^*$, is equal to the inverse of the average spacing between antiphase boundaries. This suggests the presence of a translation interface normal to the a axis every two unit cells. Figure 2 proposes an example of an ordered domain, which is able to explain the observed distribution of split diffuse scattering maxima. The iodine chains form ribbons running parallel to the a axis comprising zig-zag motifs. The SRO scattering arises from the presence in the host material of this kind of ordered domain, which can be more or less elongated in the direction of the a axis.

The presence of diffuse scattering implies not only the absence of periodicity along the b axis, along which the linear I_3^- ions are randomly distributed, but also that ordered domains are not strongly correlated to each other along the c axis. This is not surprising due to the distance between iodine layers (1.89 nm). The SRO of iodine has essentially a two-dimensional character.

The dark-field micrographs taken with the SRO diffuse scattering confirm the existence of ordered microregions sprinkled through the sample. However, the image interpretation is difficult because of the weakness of the diffuse maxima, the overlap of domains and the dynamical diffraction effects.

Electron diffraction: Long-range-order superlattice reflections

In the same sample, there are sporadic areas whose [001] zone axis diffraction pattern contains a number of extra spots that reveal a long-range ordering of the linear I_3^- ions, instead of SRO diffuse scattering. Figure 3 shows that the extra reflections can be attributed to two identical lattices related to each other by a 90° rotation

about the c axis. The two variants are based on $(\frac{1}{2}a\sqrt{2}, a\sqrt{2}, c)$ and $(a\sqrt{2}, \frac{1}{2}a\sqrt{2}, c)$ unit cells, respectively. In fact, the basic spots 110 and $\bar{1}10$ correspond to the reflections 100 and 020 of the first variant and to the reflections 200 and 010 of the second, respectively. The superlattice spots that do not correspond to any basic reflection are split. They are typical of crystals containing a periodic array of antiphase boundaries and, more precisely, of translation interfaces characterized by a translation vector equal to half a lattice parameter (see Appendix B for more details). Variant I exhibits antiphase boundaries characterized by the translation vector $\frac{1}{2}$ [010], which corresponds to the translation vector $\frac{1}{2}$ [110] in the basic crystal, and which splits the spots along rows corresponding to odd values of k. Analogously, in variant II the translation vector is $\frac{1}{2}$ [100], or $\frac{1}{2}$ [$\bar{1}$10] in the basic crystal, and the spots split if h is odd. In both cases the translation corresponds to a $\frac{1}{2}a\sqrt{2}$ displacement, along [110] and [$\bar{1}$10] directions of the basic structure, respectively. A very important point is that the distance between split spots is about five times smaller than the reciprocal vector corresponding to 110: this

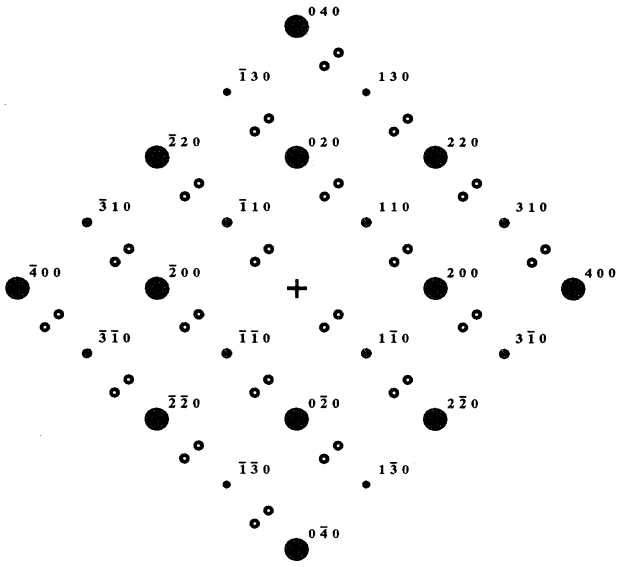

Variant I

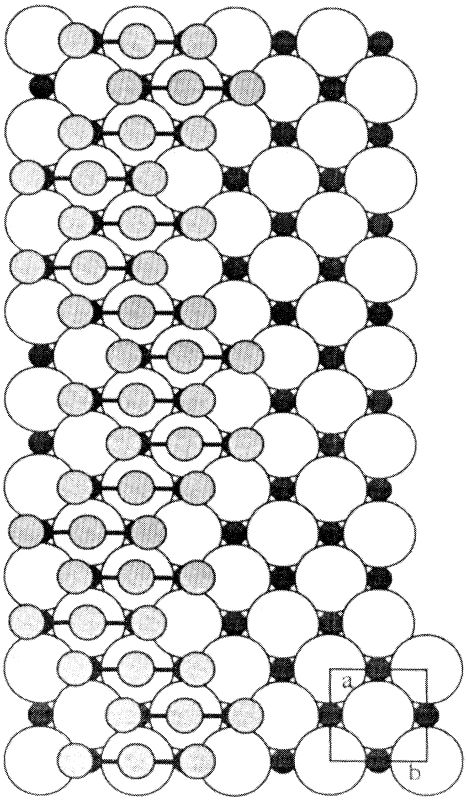

FIG. 2. A structural model showing the configuration of I_3^- ions relative to the bismuth and the oxygen atoms (small black and large light gray circles, respectively) in the underlying BiO layer, which is able to explain the observed distribution of diffuse scattering (Fig. 1). The iodine chains form bidimensional ribbons parallel to the a axis constituted of zig-zag motifs due to the presence of antiphase boundaries, normal to this direction, every two unit cells.

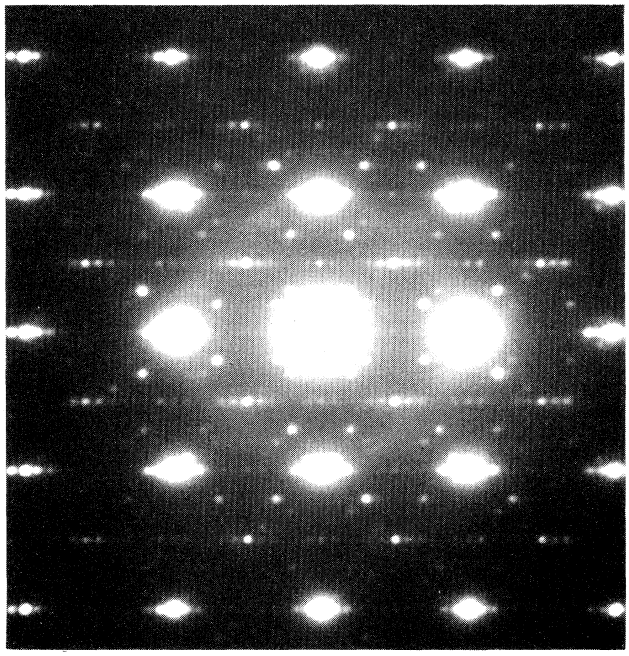

FIG. 3. [001] zone axis diffraction pattern observed in a single crystal of the I-Bi2212 compound. The pattern shows sharp superlattice spots instead of the diffuse scattering intensities of Fig. 1, and can be attributed to two identical lattices related to each other by a 90° rotation about the c axis, as shown in the simulation. Small open circles refer to the superlattice spots that do not correspond to any reflection of the basic crystal (indexed black circles), and are split. The basic spots 110 and $\bar{1}$10 correspond to the reflections 100 and 020 of the first variant and to the reflections 200 and 010 of the second one, respectively. The splitting is typical of crystals containing a periodic array of antiphase boundaries as explained in Appendix B.

means that the average distance between adjacent antiphase boundaries is about $2.5a\sqrt{2}$. It should be noted that the structural modulation periodicity is about five times the lattice parameter b, indicating the possibility of a correlation between iodine long-range order and the modulation.

A model of the superlattice due to iodine chain ordering is illustrated in Fig. 4. Antiphase boundaries and several superlattice unit cells showing the translation of adjacent domains are underlined. This model is consistent with the measured composition, the conclusions drawn from the diffuse scattering observations, and the geometry of the experimental diffraction pattern. Because of the complexity of the host crystal, we did not attempt to calculate the observed intensities. The ordering of iodine chains along the two diagonals of the basic unit cell is equivalent. For this reason, two variants of the superlattice, perpendicular to each other, coexist in the sample. Furthermore, they are intermixed because we have never observed a diffraction pattern containing only one variant. Unfortunately, we were unable to estimate the extent of the long-range-ordered regions because they were only observed in very small areas protruding from thicker flakes.

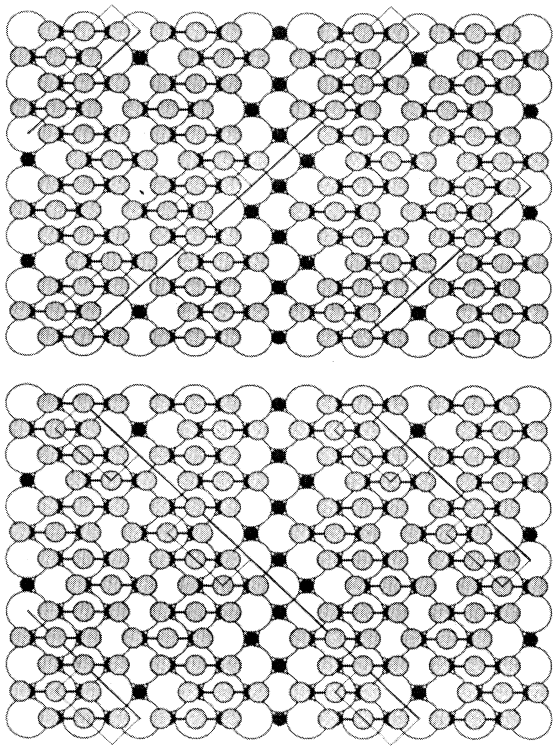

FIG. 4. Structural models showing the long-range order of I_3^- ions relative to the bismuth and the oxygen atoms (small black and large light gray circles, respectively) in the underlying BiO layer, corresponding to the two variants of the superlattice observed in the diffraction pattern reported in Fig. 3. The antiphase boundaries and a few superlattice unit cells showing the translation between adjacent domains are marked. Regions with high concentration of iodine alternate with regions of lower content with a periodicity of about 5**b**, like the structural modulation of the basic crystal.

The model suggested in Fig. 4 shows iodine-rich and -poor regions alternating with a periodicity of about 5**b**, like the structural modulation of the basic crystal. The connection between structural modulation and iodine concentration is clear in HREM observations taken with the [100] incidence (Fig. 6 of Ref. 3 and Fig. 1f of Ref. 4), especially if compared with the corresponding image of the nonintercalated material (Fig. 3 of Ref. 16). Iodine seems more concentrated in the wider regions between the BiO layers created by the modulation, enhancing in this way the effect of the modulation on the micrographs. The interpretation of Chenevier, Ikeda, and Kadowaki[4] is based on alternation of I-concentrated and I-deficient regions creating building blocks along the b-axis whose length is six and seven times $\frac{1}{2}a\sqrt{2}$, which is approximately the distance of the periodicity of the modulation. It seems that the modulation of the host crystal causes constrictions in the location of the iodine chains. This explains why the local arrangements of iodine chains have a ribbon morphology with a narrow width along the b-direction.

High-resolution electron microscopy

Our HREM observations concern only the [001] zone axis, an orientation that has not been studied before to our knowledge. The high-resolution image of Fig. 5 shows a typical aspect of I-Bi2212 single crystals along the c axis. This zone axis is particularly relevant because along this direction the heavy atoms of the host crystal form columns that appear as white or black dots, depending on the specimen thickness. Therefore, it is possible to get structural information even without image simulation.

Figure 5 shows that the crystal is not perfect but consists of small domains, which are more evident in the thinnest region of the sample near the edge (top of the micrograph). This is a direct consequence of the intercalation process. In fact, the $\frac{1}{2}a$ staggered stacking of basic blocks of one molecular unit, bounded by BiO planes, of the Bi2212 parent structure becomes a commonly registered stacking sequence in the intercalated materials. Therefore, a new crystal contains only one basic block per unit cell instead of two, and they are connected by symmetrical BiO-I-BiO triplet layers, where the Bi atoms in one layer are sited directly above the Bi atoms in the second layer.[17] The required shift of $\frac{1}{2}a$ of one basic block with respect to another in order to realign the BiO layers surrounding the iodine does not take place simultaneously throughout the crystal, and so induces the formation of domains related to each other by a translation $\frac{1}{2}a$, with the creation of defects between them as shown in Fig. 6. This image was obtained by filtering the experimental micrograph, i.e., by keeping the reflections of the host material and eliminating the diffuse scattering due to the iodine and the noise from the diffraction pattern.

Figure 5 shows also another kind of disorder of the basic structure in the thicker part of the foil (bottom right). A different kind of contrast is present, locally, in

small regions elongated in the direction of the *a* axis. We interpret this contrast as having its origin in the diffuse scattering due to the short-range order of iodine linear chains. Specifically, the presence in the micrograph of bright white dots forming a square pattern along the diagonals of the host unit cell is related to the presence of individual iodine chains without any hypothesis about their mutual location in different layers, as shown by the image simulation inset in Fig. 5. The model used here, detailed in Table I, corresponds to the host material with a random distribution of iodine chains parallel to the *b* axis; this diagonal pattern cannot be simulated with models based on atomic iodine, sitting at regular lattice positions,[3] nor with the nonintercalated crystal.

We did not try to simulate other kinds of contrast present in Fig. 5 because of the large number of possible models corresponding to the several configurations of iodine chains in an individual ribbon and the variety of spatial combinations of ribbons. Although the interaction between chains located in the same ribbon is sufficiently strong to create an ordered domain, the interaction is very weak for chains in different ribbons. For this reason, we cannot obtain direct information about the three-dimensional localized ordering of iodine. It should be noted that the size and the number of ordered islands shown by the HREM image does not necessarily correspond to those of the actual domains. In fact, the origin of the HREM contrast is related to the composition and periodicity of the atomic columns parallel to the direction of observation, whose projection constitutes the image.

Further simulations have demonstrated that the present model involving molecular I_3^- ions is also consistent with the HREM observations of Kijima *et al.*[3] along the [010] and [1$\bar{1}$0] zone axes. In fact, an improved matching of the simulated and experimental images can be achieved by imposing on the iodine chains a slight tilt in the *c*-axis direction. Such a tilt seems likely due to the large separation of facing BiO layers, especially considering the real positions of atoms imposed by the structural modulation,[11] and also due to the length of the I_3^- molecules slightly exceeding the spacing of Bi atoms. However, the chains cannot be tilted more than 12° because of the large iodine ionic radius. It should be noted

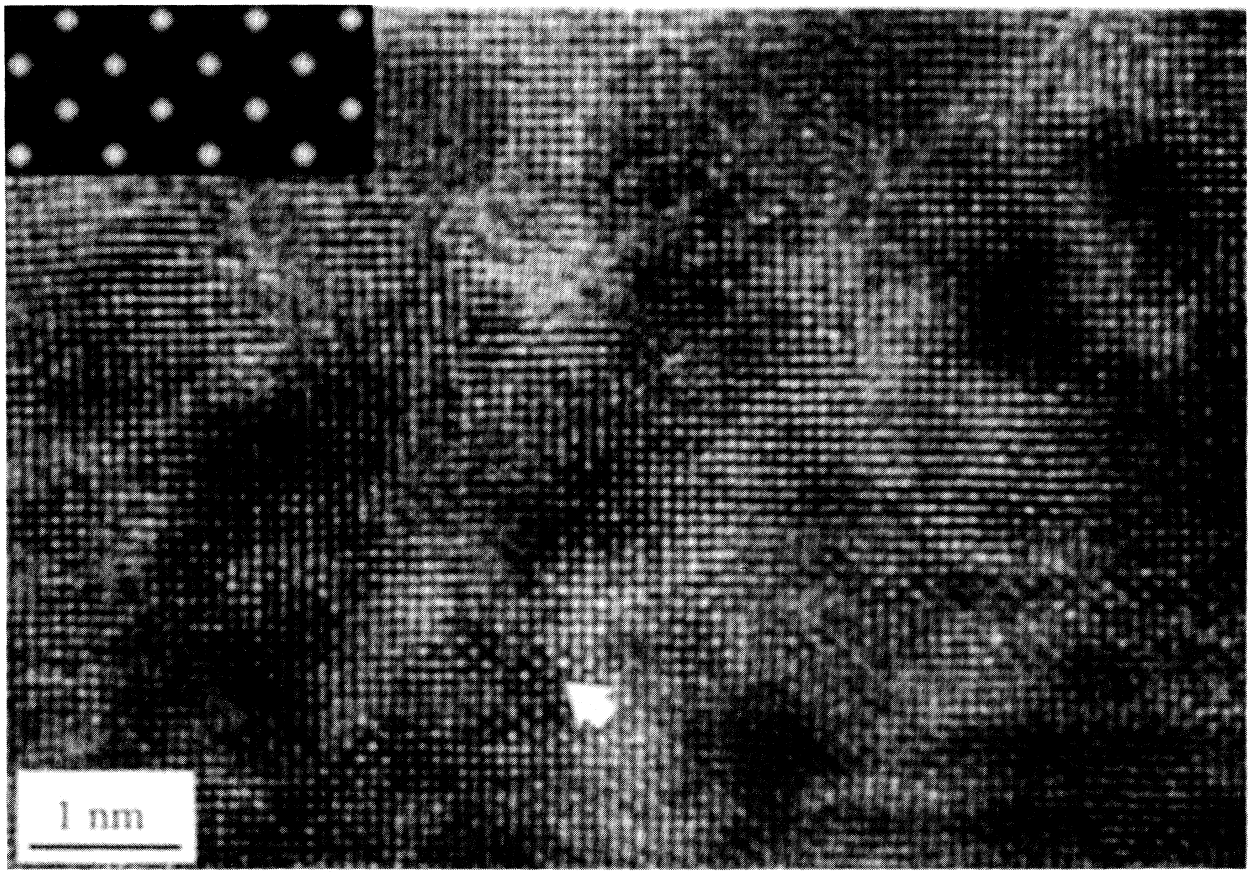

FIG. 5. High-resolution electron microscopy image showing a typical aspect of I-Bi2212 single crystals along the *c* axis. Small domains interconnected by planar defects are visible in the thinnest region (top of the micrograph). In the thicker part of the sample (bottom right) a different kind of contrast is present, locally, in small regions elongated in the direction of the *a* axis, which is horizontal in this micrograph. The particular contrast arrowed, whose simulation is shown in the inset, corresponds to the presence of a random distribution of individual iodine chains. The calculated image refers to a thickness of about 7.5 nm and to the Scherzer defocus (−60 nm).

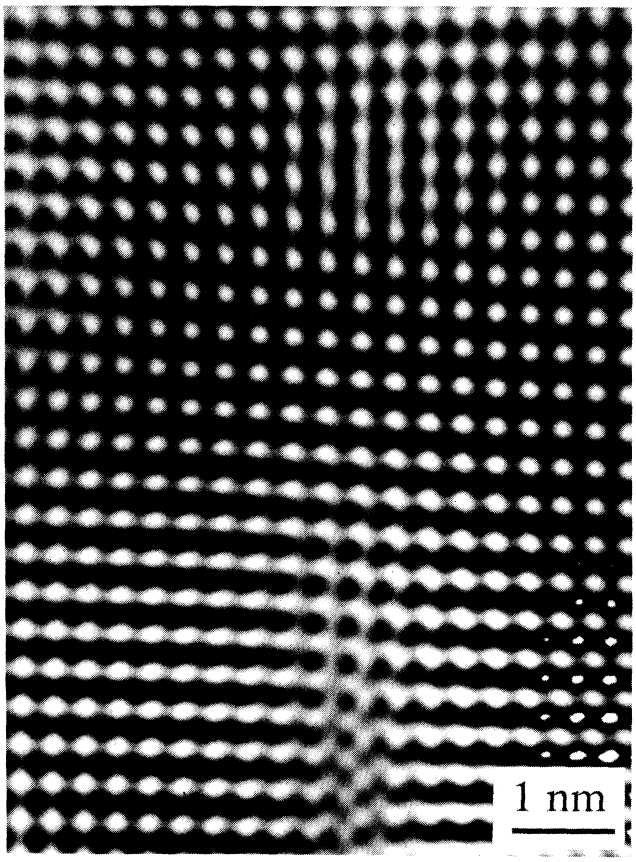

FIG. 6. Filtered image obtained by masking the diffraction pattern corresponding to the image reported in Fig. 5 in order to improve the contrast due to the host material. Defects created in accommodating the presence of domains staggered by $\frac{1}{2}a$ due to the realignment of BiO layers adjacent to iodine are evident.

though, that a very similar contrast can be obtained by reducing the chain tilt and introducing instead a modulation on the z coordinate of the Bi atoms stronger than that in the parent phase. This would be consistent with the apparently enhanced modulation discussed earlier. With either the iodine chain tilt, or the increased Bi positional modulation, the achieved contrast is in good agreement with the experimental contrast. Even the displacement of a few atoms can produce an effect on the HREM images because I and Bi are both strong electron scatters. Moreover, the contribution to scattering intensities of one atom of bismuth is about 70% stronger than that of one atom of iodine.[18]

IV. CONCLUSION

Electron diffraction and high-resolution electron microscopy observations along [001] of Bi2212 after iodine intercalation have shown that iodine is present as I_3^- linear molecules in agreement with Raman studies. I_3^- units are all parallel to the b axis with the central atom between two oxygen atoms of facing BiO layers, and with the two atoms at the ends of the chain slightly displaced in the b direction with respect to the opposing bismuth atoms (because the chain length is about 0.05 nm longer than the lattice parameter of the host material). The short-range and long-range ordering of the triiodide ion chains produce domains of ordered phases characterized by different antiphase boundaries. The structural model suggested is not only consistent with our present observations but reconciles previous results.

TABLE I. Crystallographic data, atomic parameters and site occupancy for the I-Bi2212 phase containing a random distribution of iodine chains parallel to the b axis. The atomic sites have been calculated from the corresponding atomic positions in the average structure of the parent phase (Ref. 11). A triclinic unit cell was chosen because no information is available about the symmetry of the intercalated material. The positions of the iodine atoms belonging to the individual I_3^- units have been determined by siting the chain-center iodine atom between two opposing oxygen atoms. The correct composition was imposed by attributing to each iodine site a suitable occupancy parameter. Crystal $IBi_2Sr_2CaCu_2O_x$ configurations are $a=0.54$ nm, $b=0.54$ nm, $c=1.89$ nm, alpha=90.00 deg, beta=90.00 deg, gamma=90.00 deg, triclinic system, and a primitive Bravais lattice.

	Atoms coordinates			
Element	x/a	y/b	z/c	Occupancy
I	0.250	0.250	0.000	0.50
I	0.750	0.254	0.000	0.25
I	0.750	0.246	0.000	0.25
I	0.750	0.750	0.000	0.50
I	0.250	0.754	0.000	0.25
I	0.250	0.746	0.000	0.25
O	0.280	0.250	0.175	1.00
O	0.720	0.750	0.175	1.00
O	0.750	0.250	0.284	1.00
O	0.250	0.750	0.284	1.00
O	0.000	0.000	0.413	1.00
O	0.500	0.000	0.413	1.00
O	0.000	0.500	0.413	1.00
O	0.500	0.500	0.413	1.00
O	0.000	0.000	0.587	1.00
O	0.500	0.000	0.587	1.00
O	0.000	0.500	0.587	1.00
O	0.500	0.500	0.587	1.00
O	0.750	0.250	0.716	1.00
O	0.250	0.750	0.716	1.00
O	0.220	0.250	0.825	1.00
O	0.780	0.750	0.825	1.00
Bi	0.780	0.250	0.175	1.00
Bi	0.220	0.750	0.175	1.00
Bi	0.720	0.250	0.825	1.00
Bi	0.280	0.750	0.825	1.00
Sr	0.250	0.250	0.323	1.00
Sr	0.750	0.750	0.323	1.00
Sr	0.250	0.250	0.677	1.00
Sr	0.750	0.750	0.677	1.00
Cu	0.750	0.250	0.413	1.00
Cu	0.250	0.750	0.413	1.00
Cu	0.750	0.250	0.587	1.00
Cu	0.250	0.750	0.587	1.00
Ca	0.250	0.250	0.500	1.00
Ca	0.750	0.750	0.500	1.00

ACKNOWLEDGMENTS

The authors are indebted to Dr. J. L. Tallon of the New Zealand Institute for Industrial Research, Lower Hutt, and to Dr. H. J. Trodahl of Victoria University of Wellington, New Zealand, for helpful discussions and encouragement. We express sincere gratitude to Dr. Ph. A. Buffat, Dr. P. A. Stadelmann, and Professor L. Zuppiroli of the Ecole Polytechnique Fédérale de Lausanne, for their hospitality and assistance. We would like to thank Dr. Z. Hiroi of Kyoto University, Dr. Y. Matsui of NIRIM, and Y. Kotaka of Tokyo University, Japan, for useful discussions and corroborating experimental investigations. The assistance of the Electron Microscopy Facility of Victoria University of Wellington for the filtering operation is also appreciated.

APPENDIX A: DIFFUSE SCATTERING DUE TO A RANDOM DISTRIBUTION OF LINEAR I_3^- IONS

Following the formulation of the diffraction problem for imperfect crystals suggested by Guinier[19] and Cowley,[20] the scattering intensity I of the disordered crystal that exhibits an average periodic lattice can be considered the sum of the intensity diffracted by a perfect crystal corresponding to the average structure I_1 (sharp Bragg reflections at the reciprocal lattice nodes) and of the scattering due to the deviations from the average structure I_2 (diffuse scattering in between the reciprocal lattice nodes)

$$I=I_1+I_2=|\langle F\rangle|^2+|\Delta F|^2 ,$$

where $\langle F\rangle$ and ΔF are the Fourier transform of the electronic density distribution of the average lattice $\langle\rho(\mathbf{r})\rangle$ and of the deviation from the average lattice $\Delta\rho(\mathbf{r})$, respectively. In other words, the intensity of diffuse scattering I_2 is the Fourier transform of the Patterson function of the deviation from the average structure $\Delta\rho(\mathbf{r})*\Delta\rho(\mathbf{r})$.

The diffuse scattering observed in the pattern of Fig. 1 due to the disorder created by the presence of a random distribution of linear iodine units in the Bi2212 crystal can be analyzed from this point of view. The diffuse scattering distribution corresponds to periodic functions, whose period is $2L^{-1}$ (L is the length of linear I_3^- ions), with maxima at $u=(2n+1)L^{-1}$ in the diffraction pattern rows corresponding to $h=2n$ and inversely at $u=2nL^{-1}$ if $h=2n+1$ (where u is the reciprocal lattice variable along the b^* axis and h the conventional Miller index). We will first treat the diffuse scattering distribution corresponding to $h=0$ and then explain its behavior elsewhere.

Since the I_3^- ions are linear and the observed diffuse scattering is along the direction of the b^* axis, we consider a monodimensional model of the problem as illustrated in Fig. 7. The Patterson peaks correspond to the possible distances between scattering centers, in our case the iodine atoms of the I_3^- ions in which the characteristic distances are $0, \frac{1}{2}L$ and L. The Fourier transform of this function contains two periodic components, one corresponding to a period $2L^{-1}$ and the other to a period L^{-1},

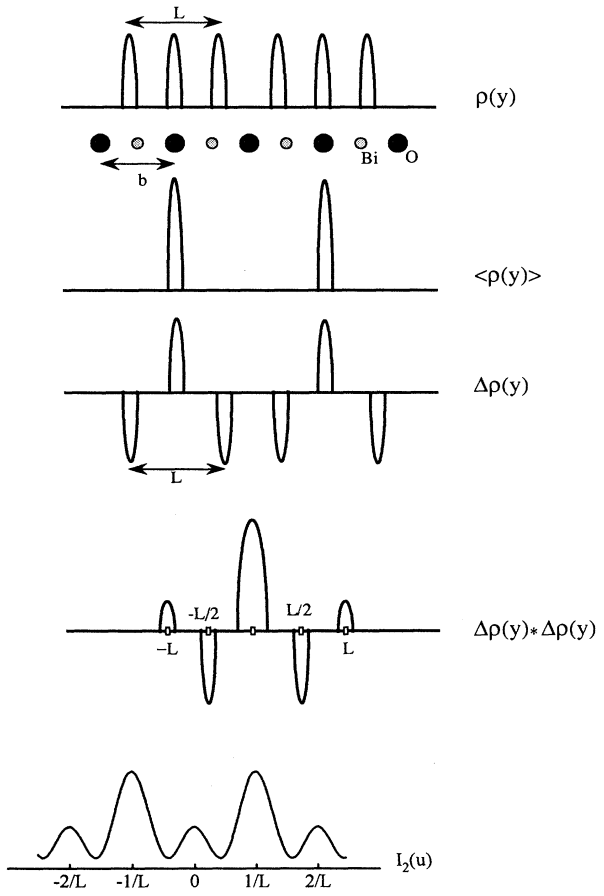

FIG. 7. Monodimensional diagrams representing the electron density distribution $\rho(\mathbf{r})$ related to the presence of iodine chains, the periodic average structure $\langle\rho(\mathbf{r})\rangle$, the deviation from the average structure $\Delta\rho(\mathbf{r})$, the Patterson function $\Delta\rho(\mathbf{r})*\Delta\rho(\mathbf{r})$, and its Fourier transform corresponding to the diffuse scattering.

which could be expressed as

$$I_2=I_{2o}(1-\cos\pi Lu+\tfrac{1}{2}\cos 2\pi Lu) ,$$

as shown in Fig. 7.

The main maxima of this function correspond to those of the observed diffuse scattering corresponding to $h=2n$ (Fig. 1). This function can describe the diffuse scattering intensity observed when $h=2n+1$ if a shift of half a period is introduced. This effect can be seen as a sort of extinction that arises because the bidimensional arrangement of iodine chains in the a-b plane is characterized by the translation $\frac{1}{2}[110]$.

APPENDIX B: DIFFRACTION EFFECTS DUE TO A PERIODIC ARRAY OF TRANSLATION INTERFACES

The kinematical diffraction theory can be used to calculate the diffraction pattern of a crystal containing translation interfaces.[21] We will consider only the simple case of a periodic arrangement of translation variants related to each other by a translation corresponding to a displacement vector $\mathbf{R}$ parallel to the interface and equal

to half a lattice parameter. The first example in Fig. 8 corresponds to the variant I of the iodine superlattice (Fig. 3) and shows that the faulted structure consists of a sequence of finite slabs of crystal. Each slab contains n lattice planes $\mathbf{H}_{100}$, giving a width $D=nd_{100}$, and with a displacement vector $\mathbf{R}$ equal to $\frac{1}{2}[010]$.

To obtain the diffraction pattern of this structure we need to calculate the Fourier transform of the lattice potential. Let us assume that within a slab the lattice potential corresponds to the potential of a perfect crystal that can be represented by the Fourier series

$$V(\mathbf{r})=\sum_{\mathbf{H}} V_{\mathbf{H}} e^{2\pi i \mathbf{H}\mathbf{r}}$$

with the sum extended over the reciprocal lattice. The lattice potential of the faulted crystal can be written as the sum of the potential of each slab. Since there are two kinds of slabs, I and II, the lattice potential can be represented as:

$$V_F(\mathbf{r})=V_1(\mathbf{r})+V_2(\mathbf{r}) ,$$

where $V_1(\mathbf{r})$ and $V_2(\mathbf{r})$ are the potentials of the slabs I and II, respectively, and can be represented as follows:

$$V_1(\mathbf{r})=V(\mathbf{r})U(x)$$

with $U(x)=1$ for $nD \le x \le (n+1)D$ and zero elsewhere, and

$$V_2(\mathbf{r})=V[\mathbf{r}-(\mathbf{D}+\mathbf{R})]U(x-D) ,$$

where $\mathbf{D}+\mathbf{R}$ is the translation between the origin of part I and the corresponding origin of part II. The lattice potential of the crystal containing the translation interfaces is then

$$V_F(\mathbf{r})=V(\mathbf{r})U(x)+V[\mathbf{r}-(\mathbf{D}+\mathbf{R})]U(x-D) .$$

The Fourier transform $F(\mathbf{g})$ of $V_F(\mathbf{r})$ is the sum of $F_1(\mathbf{g})$ and $F_2(\mathbf{g})$, the Fourier transforms of $V_1(\mathbf{r})$ and $V_2(\mathbf{r})$, respectively:

$$F(\mathbf{g})=F_1(\mathbf{g})+F_2(\mathbf{g})$$

with

$$F_1(\mathbf{g})=F(\mathbf{g})*U(\mathbf{g}-\mathbf{H})=\sum_{\mathbf{H}} V_{\mathbf{H}} U(\mathbf{g}-\mathbf{H})$$

and

$$F_2(\mathbf{g})=F_1(\mathbf{g})e^{-2\pi i(\mathbf{D}+\mathbf{R})\mathbf{g}}=\sum_{\mathbf{H}} V_{\mathbf{H}} U(\mathbf{g}-\mathbf{H})e^{-2\pi i(\mathbf{D}+\mathbf{R})\mathbf{g}} .$$

Note that $\mathbf{H}$ and $\mathbf{g}$ are both vectors of the reciprocal lattice: $\mathbf{H}$ corresponds to the reflections of the perfect crystal (basic spots), whereas $\mathbf{g}$ corresponds to the reflections of the faulted lattice (superlattice spots, Fig. 8). The presence of the translation interfaces affects the intensity of a series of basis reflections which split into two superlattice spots. In order to see this, let us consider the amplitude $A_{\mathbf{H}}(\mathbf{g})$ of a generic Bragg reflection $\mathbf{H}$:

$$A_{\mathbf{H}}(\mathbf{g})=V_{\mathbf{H}}U(\mathbf{g}-\mathbf{H})[1+e^{-2\pi i(\mathbf{D}+\mathbf{R})\mathbf{g}}] .$$

Figure 8 shows that in the reciprocal lattice the u axis is perpendicular to the translation interfaces and that $\mathbf{g}-\mathbf{H}=\mathbf{u}=u\mathbf{e}_u$, so that

$$A_{\mathbf{H}}(\mathbf{g})=V_{\mathbf{H}}U(\mathbf{g}-\mathbf{H})\{1+\exp[-2\pi i(\mathbf{D}+\mathbf{R})(\mathbf{H}+u\mathbf{e}_u)]\}$$

with

$$(\mathbf{D}+\mathbf{R})(\mathbf{H}+u\mathbf{e}_u)=\mathbf{H}\mathbf{D}+uD+n$$

with n an integer. Using the explicit expression of the function U, the amplitude of the reflection $\mathbf{H}$ becomes

$$A_{\mathbf{H}}(\mathbf{g})=V_{\mathbf{H}}\exp\left[-\pi i u D\frac{\sin\pi uD}{\pi u}\right]\left[1+e^{-2\pi i(\mathbf{H}\mathbf{R}+uD)}\right] ,$$

and its intensity is then

$$I_{\mathbf{H}}(\mathbf{g})=A_{\mathbf{H}}(\mathbf{g})A_{\mathbf{H}}^{*}(\mathbf{g})=4V_{\mathbf{H}}^2\frac{\sin^2\pi uD}{(uD)^2}\cos^2\pi(\mathbf{H}\mathbf{R}+uD) .$$

The last factor determines the position of the maxima of

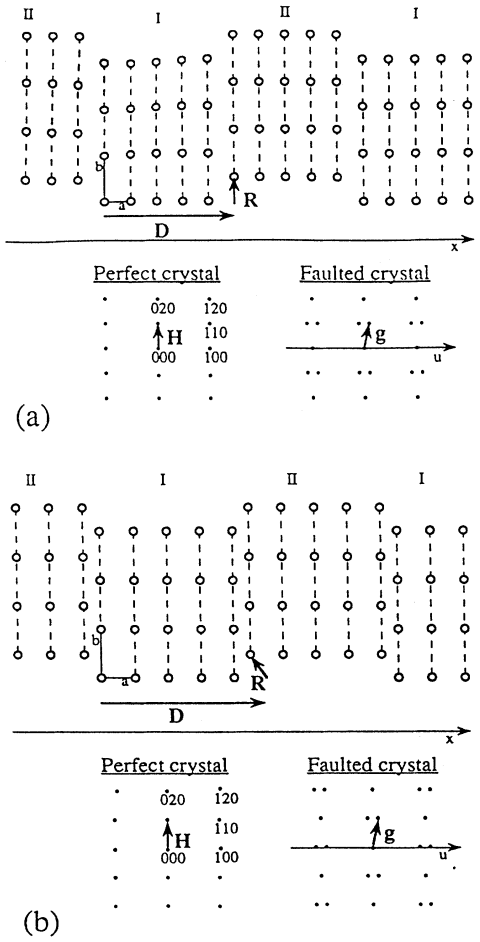

FIG. 8. Two examples of periodic arrangements of antiphase boundaries with the same orientation, but corresponding to two different displacement vectors ($\mathbf{R}=\frac{1}{2}[010]$ and $\mathbf{R}=\frac{1}{2}[110]$, respectively) and the corresponding diffraction patterns. The presence of the translation interfaces affects the intensity of a series of basic reflections that split into two superlattice spots if $\mathbf{HR}$ is half an integer. The splitting distance is the inverse of the distance between two translation interfaces and the splitting direction is perpendicular to the translation interfaces.

$I_{\mathbf{H}}(\mathbf{g})$, i.e., the position of the superlattice spots corresponding to the basic reflection **H**. This function depends on **HR** and, in our case, can have two different behaviors,

$$\cos^2\pi(\mathbf{HR}+uD)=\cos^2\pi uD \quad \text{if } \mathbf{HR} \text{ is integer ,}$$

$$\cos^2\pi(\mathbf{HR}+uD)=\sin^2\pi uD \quad \text{if } \mathbf{HR} \text{ is half integer .}$$

This means that, if **HR** is an integer, the function $I_{\mathbf{H}}(\mathbf{g})$ has a central main maximum at $u=0$, as in the case of a perfect crystal. On the other hand, if **HR** is a half integer, $I_{\mathbf{H}}(\mathbf{g})$ has two symmetrical and identical main maxima at $u=\pm(2D)^{-1}$. In this case, on the diffraction pattern the basic reflection **H** is split into two superlattice spots D^{-1} apart (corresponding to the Fig. 8). Note that D^{-1} is the inverse of the distance between two translation interfaces and that the splitting direction is perpendicular to the translation interfaces.

Figure 8 shows two different kinds of periodic arrangement of translation variants: the first is the one just treated in which the displacement vector **R** is parallel to the translation interfaces, whereas the second is a more general case, and **R** also has a component perpendicular to the interfaces (**R** is equal to $\frac{1}{2}$ [110]). The kinematical theory can be applied in the same way to this configuration and the resulting diffraction pattern will contain split spots. The splitting direction is perpendicular to the translation interfaces and does not change by changing **R**. The difference is that, in this case, other spots are split because they must correspond to a vector **H** whose scalar product with **R** is half an integer.

[1]D. Pooke, K. Kishio, T. Koga, Y. Fukuda, N. Sanada, M. Nagoshi, K. Kitazawa, and K. Yamafuji, Physica C **198**, 349 (1992).

[2]X.-D. Xiang, S. McKernan, W. A. Vareka, A. Zettl, J. L. Corkill, T. W. Barbee III, and M. L. Cohen, Nature (London) **348** 145 (1990).

[3]N. Kijima, R. Gronsky, X.-D. Xiang, W. A. Vareka, A. Zettl, J. L. Corkill, and M. L. Cohen, Physica C **181**, 18 (1991).

[4]B. Chenevier, S. Ikeda, and K. Kadowaki, Physica C **185-189**, 643 (1991).

[5]H. J. Trodahl, D. Pooke, G. J. Gainsford, and K. Kishio, Physica C **213**, 427 (1993).

[6]K. Kishio, D. Pooke, H. J. Trodahl, C. H. Subramaniam, Y. Kotaka, M. Seto, S. Kitao, and Yu. Maeda, J. Supercond. **7**, 117 (1994).

[7]N. Motohira, K. Kuwahara, T. Hasegawa, K. Kishio, and K. Kitazawa, J. Ceram. Soc. Jpn. Int. Edn. **97**, 994 (1989).

[8]P. A. Stadelmann, Ultramicrosc. **21**, 131 (1987).

[9]W. O. Saxton, T. J. Pitt, and M. Horner, Ultramicrosc. **4**, 343 (1979).

[10]D. Pooke, K. Kishio, N. Motohira, T. Tamura, T. Tomioka, T. Koga, K. Kitazawa, and K. Yamafuji, in *Advances in Superconductivity IV,* edited by H. Hayakawa and N. Koshizuka (Springer-Verlag, Tokyo, 1992), p. 233.

[11]A. Yamamoto, M. Onoda, E. Takayama-Muromachi, and F. Izumi, Phys. Rev. B **42**, 4228 (1990).

[12]E. Rosshirt, F. Frey, H. Boysen, and H. Jagodzinski, Acta Crystallogr. B **41**, 66 (1985).

[13]C. J. Schramm, R. P. Scaringe, D. R. Stojacovic, B. M. Hoffmann, J. A. Ibers, and T. J. Marks, J. Am. Chem. Soc. **102**, 6702 (1980).

[14]A. Filhol, M. Rovira, C. Hauw, J. Gaultier, D. Chasseau, and P. Dupuis, Acta Crystallogr. B **35**, 1652 (1979).

[15]H. Endres, H. J. Keller, M. Mégnamisi-Bélombé, W. Moroni, H. Pritzkow, J. Weiss, and R. Comès, Acta Crystallogr. A **32**, 954 (1976).

[16]H. Budin, O. Eibl, P. Pongratz, and P. Skalicky, Physica C **207**, 208 (1993).

[17]X.-D. Xiang, A. Zettl, W. A. Vareka, J. L. Corkill, T. W. Barbee III, and M. L. Cohen, Phys. Rev. B **43**, 11 496 (1991).

[18]J. A. Ibers and B. K. Veinshtein, *International Crystallographic Tables* (Kynoch, Birmingham, 1962), Vol. III, Tables 3.3.3A(1) and A(2).

[19]A. Guinier, *X-Ray Diffraction In Crystals, Imperfect Crystals and Amorphous Bodies* (Freeman, San Francisco, 1963), Chap. 6.

[20]J. M. Cowley, *Diffraction Physics* (North-Holland, Amsterdam, 1975), Chap. 7.

[21]J. van Landuyt, R. de Ridder, R. Gevers, and S. Amelinckx, Mater. Res. Bull. **5**, 353 (1970).

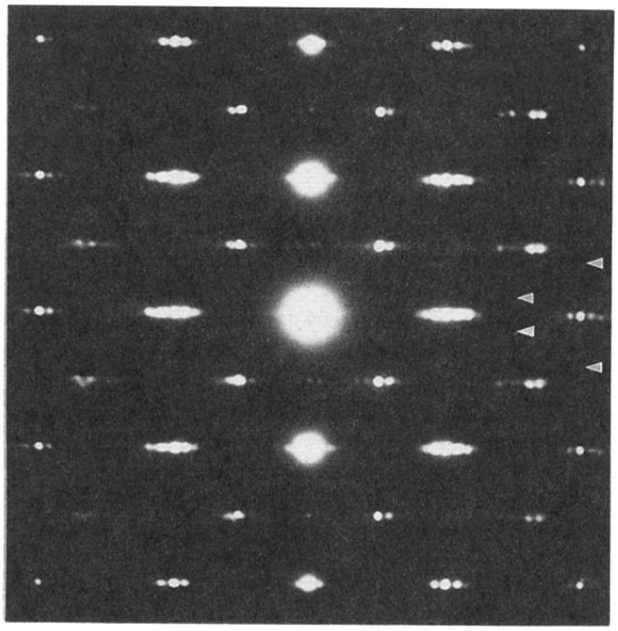

FIG. 1. Typical long-exposure [001] zone axis diffraction patterns observed in single crystals of the I-Bi2212 compound. In addition to the fundamental Bragg reflections corresponding to the crystal structure of the host material, the pattern shows a distribution of diffuse scattering intensities characterized by modulated diffuse superlattice reflections split and elongated along the direction indicated by the short arrows. The period of modulation of the diffuse streaks is $1.84\mathbf{b}^*$.

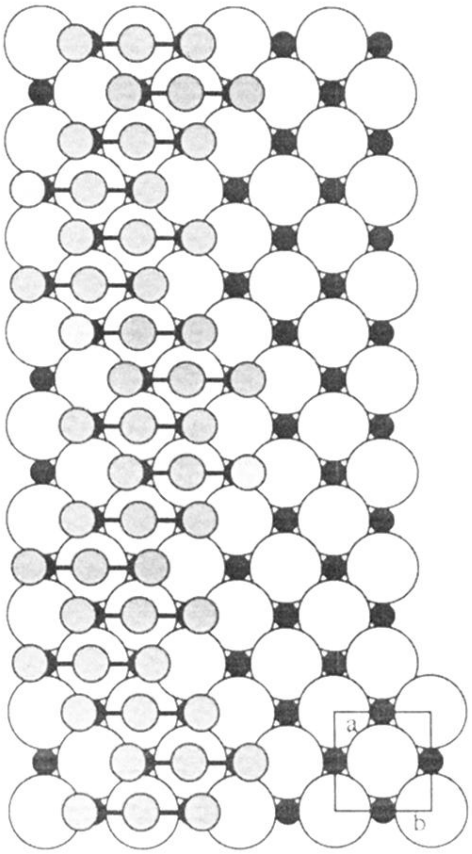

FIG. 2. A structural model showing the configuration of I_3^- ions relative to the bismuth and the oxygen atoms (small black and large light gray circles, respectively) in the underlying BiO layer, which is able to explain the observed distribution of diffuse scattering (Fig. 1). The iodine chains form bidimensional ribbons parallel to the *a* axis constituted of zig-zag motifs due to the presence of antiphase boundaries, normal to this direction, every two unit cells.

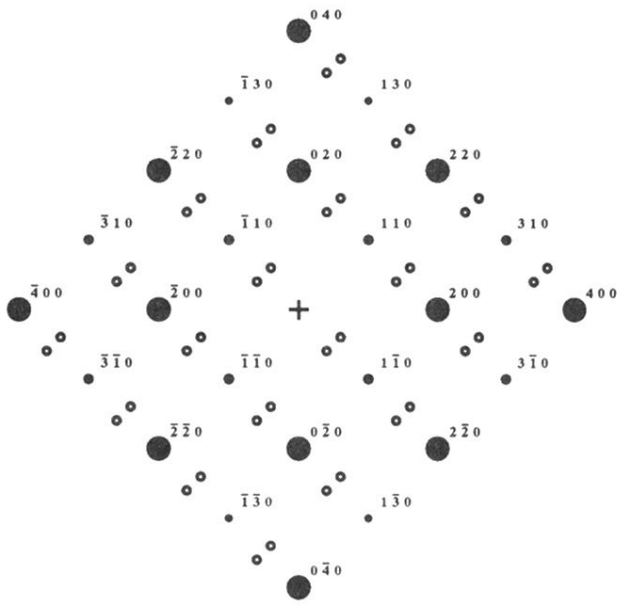

Variant I

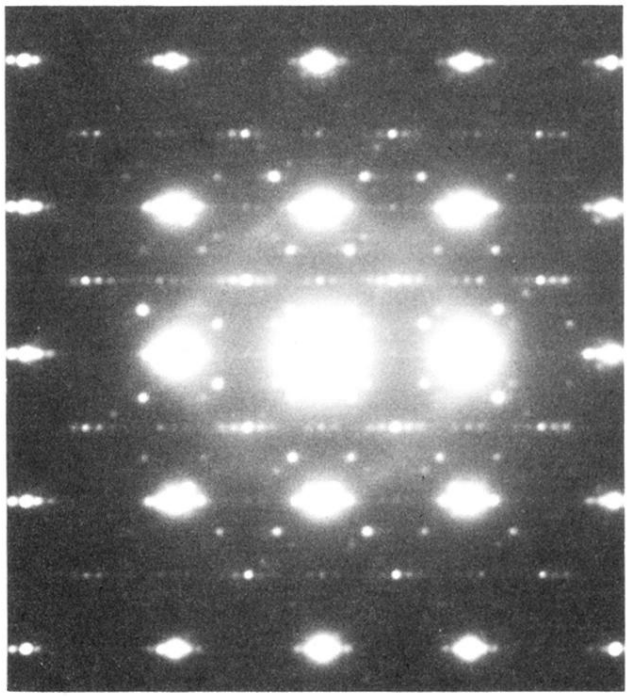

FIG. 3. [001] zone axis diffraction pattern observed in a single crystal of the I-Bi2212 compound. The pattern shows sharp superlattice spots instead of the diffuse scattering intensities of Fig. 1, and can be attributed to two identical lattices related to each other by a 90° rotation about the *c* axis, as shown in the simulation. Small open circles refer to the superlattice spots that do not correspond to any reflection of the basic crystal (indexed black circles), and are split. The basic spots 110 and $\bar{1}$10 correspond to the reflections 100 and 020 of the first variant and to the reflections 200 and 010 of the second one, respectively. The splitting is typical of crystals containing a periodic array of antiphase boundaries as explained in Appendix B.

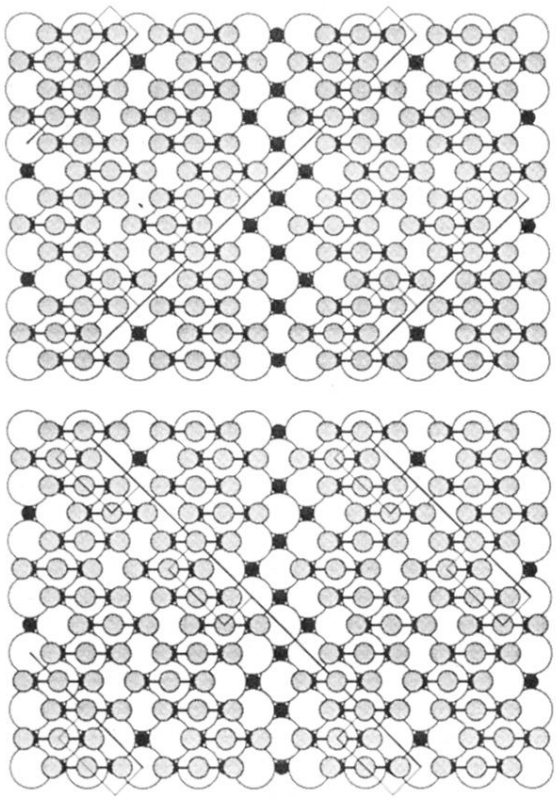

FIG. 4. Structural models showing the long-range order of I_3^- ions relative to the bismuth and the oxygen atoms (small black and large light gray circles, respectively) in the underlying BiO layer, corresponding to the two variants of the superlattice observed in the diffraction pattern reported in Fig. 3. The antiphase boundaries and a few superlattice unit cells showing the translation between adjacent domains are marked. Regions with high concentration of iodine alternate with regions of lower content with a periodicity of about 5**b**, like the structural modulation of the basic crystal.

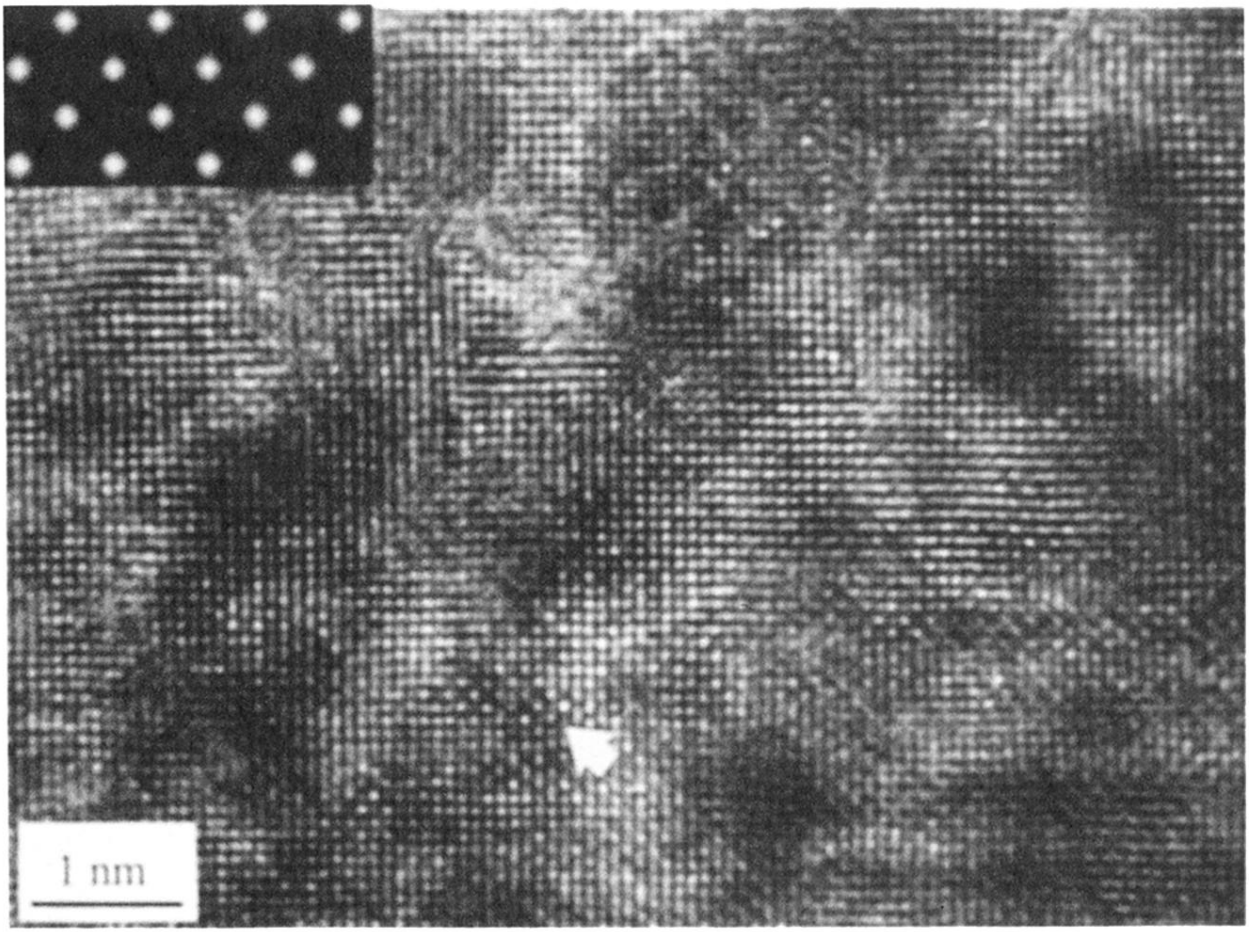

FIG. 5. High-resolution electron microscopy image showing a typical aspect of I-Bi2212 single crystals along the *c* axis. Small domains interconnected by planar defects are visible in the thinnest region (top of the micrograph). In the thicker part of the sample (bottom right) a different kind of contrast is present, locally, in small regions elongated in the direction of the *a* axis, which is horizontal in this micrograph. The particular contrast arrowed, whose simulation is shown in the inset, corresponds to the presence of a random distribution of individual iodine chains. The calculated image refers to a thickness of about 7.5 nm and to the Scherzer defocus (−60 nm).

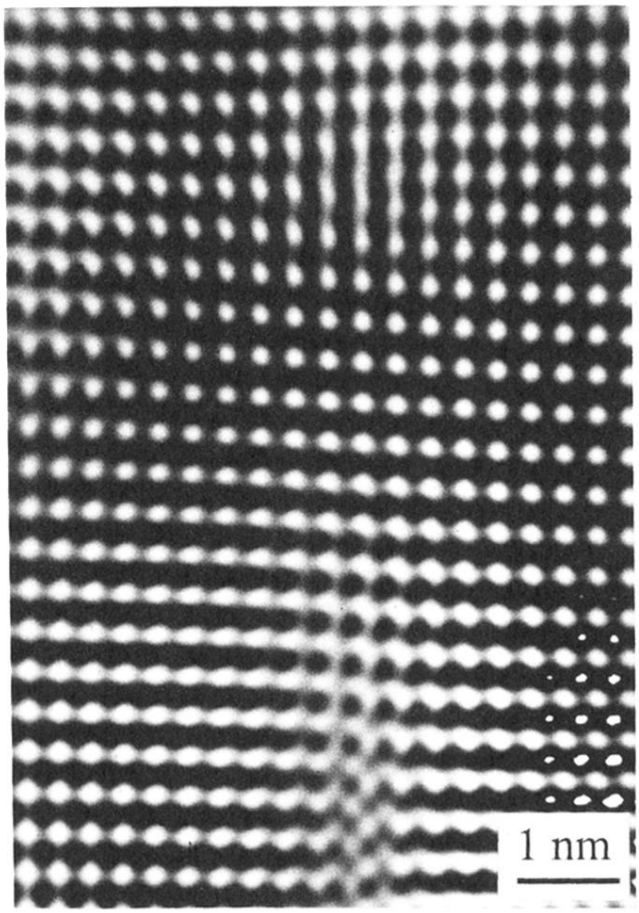

FIG. 6. Filtered image obtained by masking the diffraction pattern corresponding to the image reported in Fig. 5 in order to improve the contrast due to the host material. Defects created in accommodating the presence of domains staggered by $\frac{1}{2}a$ due to the realignment of BiO layers adjacent to iodine are evident.